Sprayable antibacterial Persian gum-silver nanoparticle dressing for wound healing acceleration

Amirsadeghi, Armin

2021-06

Amirsadeghi , A , Jafari , A , Hashemi , S-S , Kazemi , A , Ghasemi , Y , Derakhshanfar , A , Shahbazi , M-A & Niknezhad , S V 2021 , ' Sprayable antibacterial Persian gum-silver nanoparticle dressing for wound healing acceleration ' , Materials Today Communications , vol. 27 , 102225 . https://doi.org/10.1016/j.mtcomm.2021.102225

http://hdl.handle.net/10138/334464
https://doi.org/10.1016/j.mtcomm.2021.102225

Materials Today Communications 27 (2021) 102225

Contents lists available at ScienceDirect

Materials Today Communications

journal homepage: www.elsevier.com/locate/mtcomm

Sprayable antibacterial Persian gum-silver nanoparticle dressing for wound healing acceleration

Armin Amirsadeghi [a,b,1], Arman Jafari [a,1], Seyyedeh-Sara Hashemi [b,**], Aboozar Kazemi [c], Younes Ghasemi [c], Amin Derakhshanfar [d,e,f], Mohammad-Ali Shahbazi [g,h,*], Seyyed Vahid Niknezhad [b,c,**]

[a] School of Chemical and Petroleum Engineering, Shiraz University, Shiraz, 71348-51154, Iran
[b] Burn and Wound Healing Research Center, Shiraz University of Medical Sciences, Shiraz, 71345-1978, Iran
[c] Pharmaceutical Sciences Research Center, Shiraz University of Medical Sciences, Shiraz, 71345-1583, Iran
[d] Diagnostic Laboratory Sciences and Technology Research Center, School of Paramedical Sciences, Shiraz University of Medical Sciences, Shiraz, Iran
[e] Department of Comparative Biomedical Sciences, School of Advanced Medical Sciences and Technologies, Shiraz University of Medical Sciences, Shiraz, Iran
[f] Comparative and Experimental Medicine Center, Shiraz University of Medical Sciences, Shiraz, Iran
[g] Drug Research Program, Division of Pharmaceutical Chemistry and Technology, Faculty of Pharmacy, University of Helsinki, Helsinki, FI-00014, Finland
[h] Zanjan Pharmaceutical Nanotechnology Research Center (ZPNRC), Zanjan University of Medical Sciences, Zanjan, 45139-56184, Iran

ARTICLE INFO

Keywords:
Persian gum
Nanoparticle
Antibacterial
Spray
Skin
Wound dressing

ABSTRACT

Wound infection is considered a significant challenge in skin injuries. Sprayable antibacterial wound dressings are interesting alternatives to their traditional counterparts because of their facile preparation, ease-of-use, and the possibility of topical delivery of antibacterial materials. Herein, novel sprayable antibacterial dressings are formulated and reported. The dressings were developed by in-situ formation of Ag-nanoparticles (Ag-NPs) using Persian gum (PG) as a carbohydrate polymer. Several tests were conducted to investigate the effect of polymer concentration on the sprayablity, biocompatibility, and antibacterial activity of the dressings (PG/Ag-NPs). Results showed that formulations up to 2 wt.% PG/Ag-NPs could be sprayed properly and form intact films. Antibacterial evaluations also showed biocidal activity of 1% PG/Ag-NPs against *Pseudomonas aeruginosa* and *Staphylococcus aureus*. Cytotoxicity and *in vivo* full-thickness wound healing evaluation confirmed that 1% PG/Ag-NPs spray was safe and improved wound healing process. All the results confirmed the high potential of formulated sprayable dressings for wound repair.

1. Introduction

Skin, the outermost organ of the human body, makes a strong defensive line against exogenous hazards [1]. Any damage to this multifunctional organ makes the human body vulnerable to microbial invasion [2]. As a result, wound infection is one of the most prevalent and challenging problems in different skin disorders, such as diabetic ulcers and burn injuries [3–5]. Wound infection can severely jeopardize human health by arising acute inflammatory response that leads to delayed wound healing [6]. Systemic antibiotic administration is a traditional method to prevent wound infection; however, the growing number of antibiotic-resistant bacteria and low efficiency of antibiotic delivery to the wound site highlight the need for new antibacterial materials as well as new methods for their topical delivery [7–9]. To tackle these problems, wound dressings containing essential oils, polymers with intrinsic antibacterial properties, and nanoparticles as alternative antibacterial agents have been developed [10–13]. Different forms of these wound dressings, such as nanofibers, films, sponges, foams, and hydrogels are currently available in the market [14,15]. However, these conventionally available wound dressings are mostly incapable of covering large and asymmetrical wounds. Besides, wound dressings need to be replaced regularly, and because they are inclined to

* Corresponding author at: Drug Research Program, Division of Pharmaceutical Chemistry and Technology, Faculty of Pharmacy, University of Helsinki, Helsinki, FI-00014, Finland.
** Corresponding authors at: Burn and Wound Healing Research Center, Shiraz University of Medical Sciences, Shiraz, 71345-1978, Iran.
E-mail addresses: Sara_hashemi@sums.ac.ir (S.-S. Hashemi), m.a.shahbazi@helsinki.fi (M.-A. Shahbazi), vahidniknezhad@sums.ac.ir (S.V. Niknezhad).
[1] Armin Amirsadeghi and Arman Jafari equally contributed to this work as first authors.

https://doi.org/10.1016/j.mtcomm.2021.102225
Received 10 October 2020; Received in revised form 3 February 2021; Accepted 28 February 2021
Available online 1 March 2021

adhere to the wound area, they are liable to cause secondary damage [16]. Consequently, engineering a wound dressing that is not only well-matched to each patient but also can be easily removed and replaced is of great interest. Recently, sprayable and injectable hydrogels and film-forming dressings have been investigated as promising alternatives to conventional dressings [17–19]. These alternatives have many advantages, including closer contact with tissue, compatibility to any asymmetrical and large wound, ease of use, and topical delivery of antibacterial agents that made them great candidates for wound healing [20–22].

Persian gum (PG) (also known as Farsi gum, Shirazi gum, Zedo gum, and Angum gum) is a carbohydrate polymer derived from the natural exudate of almond trees scattered through Zagros mountains, Iran [23]. PG has gained many applications in food industries due to its stabilizing, emulsifying, film-forming, and high water absorption properties [24–27]. However, to the best of our knowledge, its potential biomedical applications have not been reported yet.

Researches have shown that metal and metal oxide nanoparticles provide broad antimicrobial activities [28,29]. Silver nanoparticles (Ag-NPs) are among the most effective and investigated nanoparticles that have been shown to be effective against multidrug-resistant bacteria [30–33]. It has been reported that Ag-NPs' antibacterial activities are mostly derived from silver ions interaction with bacteria enzymes and proteins and/or destruction of bacteria's membrane [34,35]. However, researches have demonstrated that a high concentration of Ag-NPs could be cytotoxic to human cells due to the uptake of Ag-NPs by cells and/or reactive oxygen species (ROS) related oxidative stress [1, 36,37].

In this study, the application of PG to synthesize and stabilize Ag-NPs were investigated for the first time. A thorough characterization of the synthesized Ag-NPs embedded PG (PG/Ag-NPs) was performed. Furthermore, the potential application of PG/Ag-NPs as a sprayable antibacterial dressing for wound healing was evaluated. This research is of importance as it demonstrates the application of PG as a novel biomaterial for biomedical applications.

2. Experimental section

2.1. Materials

The natural exudate of the almond tree was obtained from the local market to be used for PG extraction. Silver nitrate ($AgNO_3$) was purchased from Sigma, USA. Commercially available spray bottles were bought from the market and used for sprayability experiments. Deionized water (DI) was used for all experiments.

2.2. Persian gum extraction

To reach water-soluble PG, almond tree exudate was dissolved in DI (5 wt.%) at 60 °C for 1 h. The resultant solution was then centrifuged at 2000 rpm for 5 min, and its supernatant was kept. Afterward, the supernatant was precipitated using 2-fold ethanol 96 % to reach the PG. PG was again dissolved in water and freeze-dried for further use.

2.3. Synthesis of silver nanoparticles embedded in Persian gum

PG was dissolved in deionized water (1.0 g to 100 mL) and heated to 60 °C. Subsequently, silver precursor, $AgNO_3$ (0.118 mmol), was added to the solution and vigorously stirred for 24 h. Then, the solution was dialyzed through SnakeSkin™ 3500 Da dialysis tubing (Thermo Scientific, USA) for two days to remove the unreacted components. The solution was further lyophilized and kept at -20 °C until use.

2.4. Characterization of PG and PG/Ag-NPs

The chemical composition of the extracted PG was initially investigated using ^{1}H nuclear magnetic resonance (^{1}H NMR). ^{1}H NMR spectra were recorded by 300 MHz Ascend™ (Bruker, Germany) using deuterium oxide (D_2O) as the solvent. Moreover, Fourier-transform infrared spectroscopy (FTIR) was used to investigate the chemical composition of extracted PG and synthesized PG/Ag-NPs using Spectrum65 (Perkin Elmer, USA). The FTIR spectra were recorded by a total number of 64 scans in the range of 400−4000 cm^{-1} and resolution of 2 cm^{-1}. Furthermore, Ultraviolet-visible (UV–vis) spectra were recorded using a spectrophotometer (UV-1280, Shimadzu, Japan) in the range of 200−800 nm to investigate the presence of Ag-NPs in the synthesized PG/Ag-NPs (0.1 % in ultra-pure water). Zeta potential analysis was also conducted using a dynamic light scattering device (SZ-100, Horiba, Japan) to investigate PG/Ag-NPs (0.1 % in ultra-pure water) surface potential value. In addition, elemental composition and elemental distribution map were taken using energy dispersive X-ray (EDX) analysis equipped in a scanning electron microscopy (SEM) device (Vega 3, TESCAN, Czech Republic). Besides, transmission electron microscopy (TEM) photographs were taken (CM120, Philips, Netherlands) to detect the Ag-NPs embedded in the PG network. Subsequently, the mean particle size and particle size distribution pattern were also calculated from TEM images by counting 50 individual nanoparticles using Digimizer software. To investigate the thermal properties, differential scanning calorimetry (DSC) and thermogravimetric analysis (TGA) analysis were performed using a thermogravimetric analyzer (TGA/DSC1, METTLER-Toledo, Switzerland). DSC and TGA analysis were performed with a 10 °C/min heating ratio and in the temperature ranges of -100 to 250 °C and 25–800 °C, respectively.

2.5. Preparation of spray solutions

Four different concentrations of spray solutions (0.5, 1, 1.5, and 2 w/v%) of PG/Ag-NPs were prepared for our investigations. For this purpose, pre-weighed amounts of PG/Ag-NPs were added to deionized water, and the mixtures were stirred at 60° overnight until PG/Ag-NPs were fully dissolved.

2.6. Rheological properties and sprayability

Rheological characteristics of the prepared solutions were investigated at room temperature (25 °C) using a rheometer apparatus (MCR-302, Anton Paar, Austria). Hysteresis analysis was performed at cyclic shear rates from 0.1 to 10^3 s^{-1} to evaluate the viscoelastic properties of the samples.

Sprayability of the prepared solutions were evaluated using conventional spray bottles (filled with 5 mL of samples). The samples were sprayed into a beaker and weighted. Each sample was sprayed for 13 times. To minimize any errors, the sprayability of each sample was repeated three times using three different spray bottles.

2.7. Film-forming properties

To evaluate PG/Ag-NPs film-forming property, the solutions were sprayed on a slide glass and dried at room temperature. The dried samples were coated with gold using a Sputtering coating device (Q150R-ES, Quorum Technologies, England), and then SEM images (Vega 3, TESCAN, Czech Republic) were taken from their surface.

2.8. Stability evaluation

The stability of spray solutions was evaluated by measuring the UV–vis spectra and pH recording over a 6-month period. For this means, solutions of all four spray concentrations (0.5, 1, 1.5, and 2% PG/Ag-NPs) were prepared, and their pH values were measured using a digital pH meter device (744, Metrohm AG, Switzerland). The prepared solutions were kept in a dark place and at room temperature, and after 3 and 6 months, the pH measurement was repeated. Moreover, the UV–vis

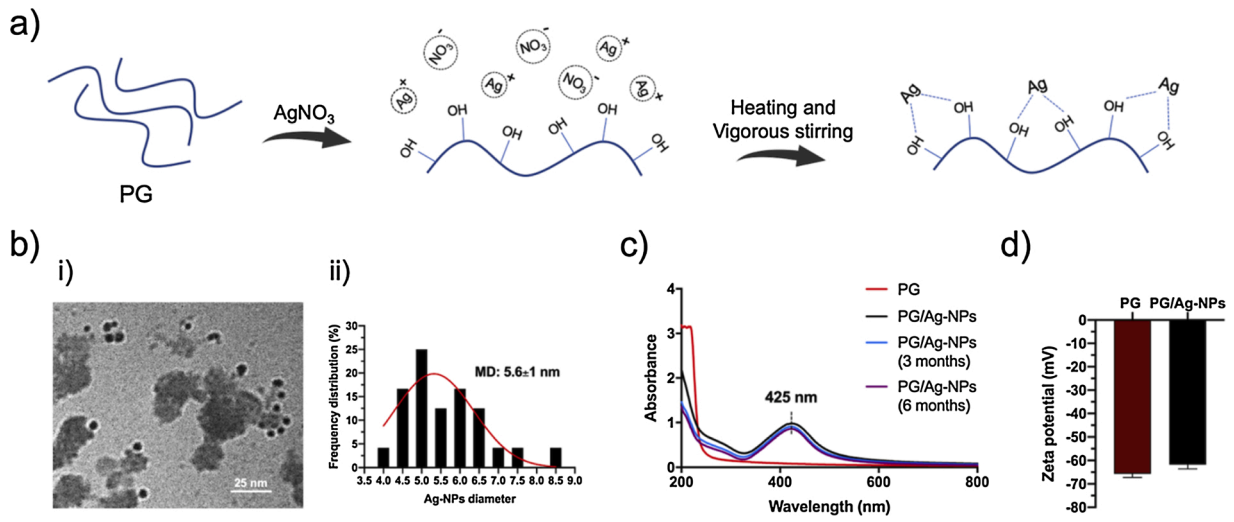

Fig. 1. (a) Schematic overview of PG/Ag-NPs synthesis, (b.i) TEM photograph of the synthesized PG/Ag-NPs and (b.ii) its derived particles mean diameter and diameter distribution pattern, (c) illustrates samples UV absorbance, and (d) showed samples zeta potential.

spectra were also recorded at these time points to compare with the previously recorded data.

2.9. Antibacterial activity

Antibacterial activity of PG/Ag-NPs against gram-positive *Staphylococcus aureus* (*S. aureus*) (ATCC 6538) and gram-negative *Pseudomonas aeruginosa* (*P. aeruginosa*) (ATCC 27853) were evaluated. Each bacterium was added into a flask filled with Mueller-Hinton broth (MHB) (Merck, Germany) and incubated at 37 °C for 24 h. After that, the bacterial suspensions were diluted to 10^6 CFU/mL.

A serial dilution assay was performed to measure the minimum inhibitory concentration (MIC). For this purpose, solutions containing 5 mg/mL PG/Ag-NPs, 0.05 mg/mL Chloramphenicol (as positive control) were prepared and added into 96-well plates. MHB solution was used for 2-fold serial dilution. Subsequently, the bacteria were added to wells and incubated at 37 °C. After 24 h, the plates were removed, and their OD at 600 nm was read using an Elisa reader (Epoch, BioTeck, USA).

Furthermore, the kinetic assay was performed to investigate the antibacterial efficiency of fabricated PG/Ag-NPs over different time intervals. A solution of 1% PG/Ag-NPs containing 10^6 CFU/mL bacteria was prepared and incubated in a shaker incubator at 37 °C and 200 rpm. After 1, 2, 3, 4, 6, and 8 h, 100 µL of each sample was taken, and their ODs at 600 nm were read. Moreover, 100 µL of each sample was taken to inoculate Muller-Hinton agar plates at each time intervals. The plates were incubated at 37 °C for 24 h, and then images were taken. All samples were prepared in MHB solution. For the control group, 10-fold dilution was performed before inoculation in agar plates.

2.10. Antioxidant and cytotoxicity properties

The antioxidant activity of PG, PG/Ag-NPs, and ascorbic acid (as standard) was investigated by the 2,2-diphenyl-1-picrylhydrazyl ($DPPH^{\bullet}$), radical scavenging assay. Therefore, 50 µL of each sample was inserted into a 96-well plate and mixed with 100 µL of DPPH solution (100 µM, dissolved in 96 % ethanol). The plate was kept in the dark place at room temperature for 40 min, and then the absorbance at 525 nm was read [38]. The radical scavenging ability (%) for all methods was quantified by using the given equation:

$$\text{Radical scavenging ability } (\%) = \left[1 - (A_i - A_j)/A_0\right] \times 100$$

Here A_i is the absorbance of the samples, Aj is the background absorbance of the samples without free radicals, and A_0 is the absorbance of the control.

To investigate the cytotoxicity of PG and synthesized PG/Ag-NPs, MTT assay was implemented. Initially, 1.5×10^4 fibroblast cells (Pasteur Institute of Iran, Iran) plus 100 µL extra culture media (DMEM-F12 supplemented with 10 % FBS and 1% pen/strep) were seeded on each well of 96-well plates. To ensure that all cells were well-attached on the culture plates, plates were incubated for 24 h at 37 °C, 90 % humidity, and 5% CO_2. After that, culture mediums were gently removed, and 400 µL UV-sterilized PG/Ag-NPs (5, 10, 15, and 20 mg/mL) solutions in culture medium were added to wells. Subsequently, the culture plates were returned into the incubator. After 24, 48, and 72 h, the culture plates were taken out from the incubator, the medium was gently removed, and 100 µL MTT solution (0.5 % MTT in cell culture medium) was added to each well. The plates were placed back into the incubator for another 4 h until formazan crystals formed. Then, the mediums were replaced with 100 µL dimethyl sulfoxide (DMSO) to dissolve the formazan crystals. Finally, the plates were put into an Elisa plate reader (Epoch, BioTeck, USA), and the OD was read at 570 and 630 nm. The cell viability was calculated compared to the control group (cell culture plate).

2.11. In vivo study

The *in vivo* wound healing test was performed under the approval of the Institutional Animal Care and Use Committee of the Shiraz University of Medical Science. For this means, twelve healthy Sprague-Dawley rats (male, 200−250 g) were first anesthetized with the combination of ketamine (100 mg/Kg) and xylazine (5 mg/Kg). Their dorsal hair was shaved, and then, two round shaped full-thickness wounds (10 mm each) were created on the back of each rat. Subsequently, one wound was treated with 1% PG/Ag-NPs solution, and the other one was left untreated (as the control group). Both wounds were then covered with petroleum gauze. After 3, 7, 10, and 14 days, the rats were anesthetized, and the image of each wound was taken for macroscopic evaluations. Moreover, three rats were sacrificed at each time interval, and the skins of wound sites were removed and fixed in 10 % formalin solution.

For the histological assay, the fixed samples were dehydrated using serially diluted alcohol solutions and put into paraffin blocks. These paraffin blocks were then sectioned and stained with hematoxylin and eosin (H&E) and Masson's trichrome. Photographs of the sections were taken by a light microscope (Olympus BX41, Japan) to evaluate the wound healing process.

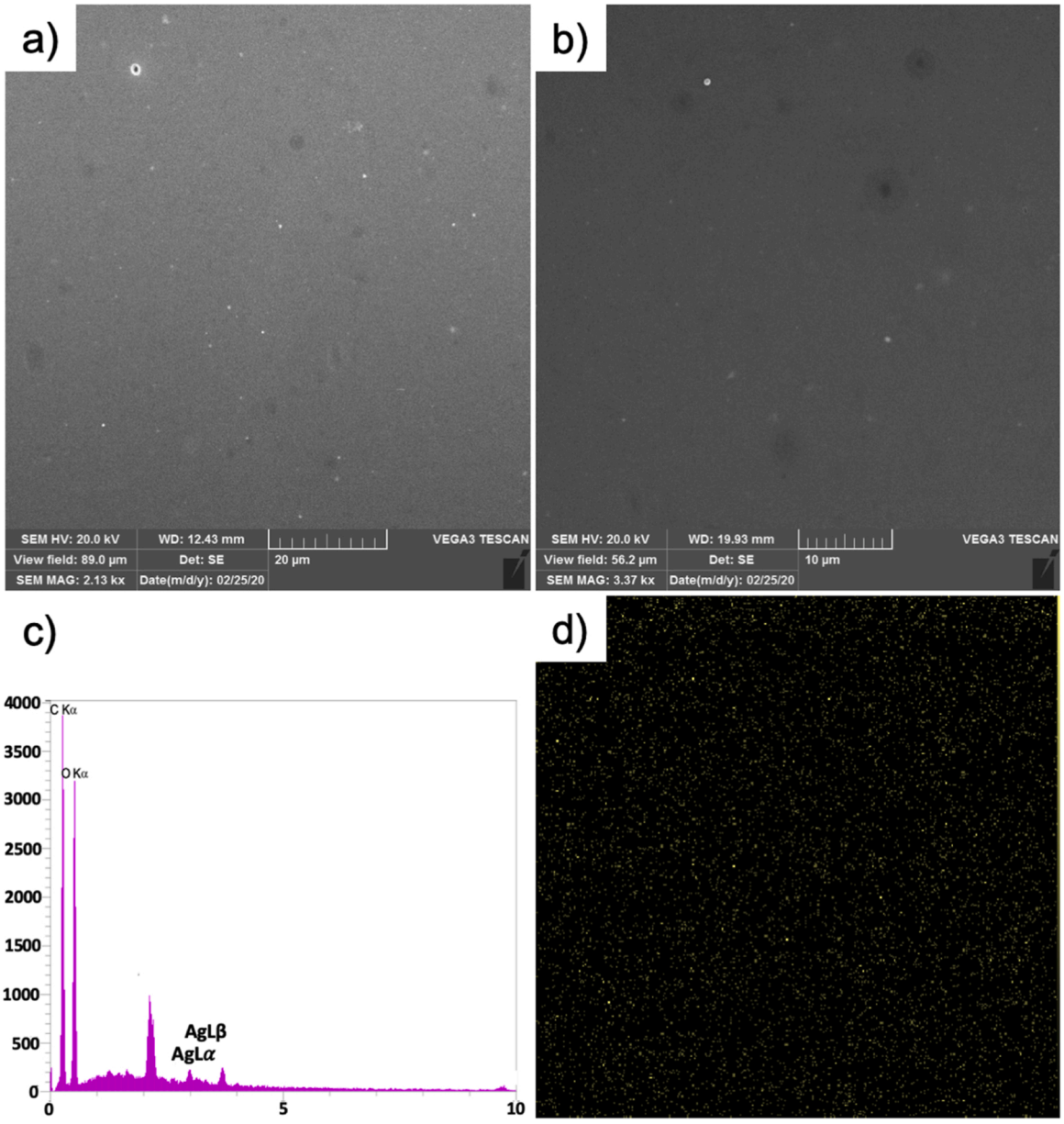

Fig. 2. SEM photograph of PG/Ag-NPs film at (a) 2.13 kX and (b) 3.37 kX; (c) EDX analysis, and (d) elemental mapping for Ag.

2.12. Statistical analysis

Statistical analysis was performed by one-way ANOVA test using GraphPad Prism 8.0 software. In this study, error bars represent mean ± standard deviation (SD) of triplicate experiments and p values lower than 0.05 considered as statistically significant with four stages (*$p < 0.05$, **$p < 0.01$, ***$p < 0.001$, and ****$p < 0.0001$).

3. Results and discussion

3.1. Characterization of PG and PG/Ag-NPs

In this study, PG was first extracted from almond trees exudes and refined to reach its soluble part. This polysaccharide not only was able to reduce Ag^{+} to Ag^{0} and form Ag-NPs without the use of any other reducing materials but also stabilized the fabricated Ag-NPs (Fig. 1a).

TEM photograph confirmed the formation of Ag nanoparticles (Fig. 1b.i) with the mean particle diameter of 5.6 ± 1.0 nm with narrow size distribution (Fig. 1b.ii). The UV–vis spectra of PG and PG/Ag-NPs were recorded in the range of 200−800 nm (Fig. 1c). For PG, no peak was observed in this range. However, for PG/Ag-NPs a peak at 425 nm appeared, which is attributed to the Ag-NPs [39,40]. Zeta potential values for PG and PG/Ag-NPs were obtained as -65.7 ± 1.5 mV and -61.8 ± 1.8 mV, respectively (Fig. 1d). Moreover, the slight shift toward more positive values in PG/Ag-NPs compared to pure PG could attribute to the electrostatic interactions between Ag-NPs and some PG negative groups [41]. Zeta potential result demonstrated that the synthesized Ag-NPs were encompassed by PG that leads to a highly stable PG/Ag-NPs suspension [42]. EDX analysis revealed that about 2% of total PG/Ag-NPs was consisted of Ag-NPs (Fig. 2c). Moreover, elemental mapping for Ag illustrated that nanoparticles were distributed uniformly through the material and did not form evident agglomerates (Fig. 2d).

^{1}H NMR spectrum of extracted PG and FTIR spectrum of extracted PG and synthesized PG/Ag-NPs were performed to evaluate their chemical composition. ^{1}H NMR spectrum of PG exhibits several peaks in the range of $\delta = 3.2–4.3$ ppm, which are attributed to protons available on hydrocarbon rings as well as a chemical shift in the range of $\delta = 1–1.1$ corresponding to methyl group protons of rhamnose. Besides, two picks

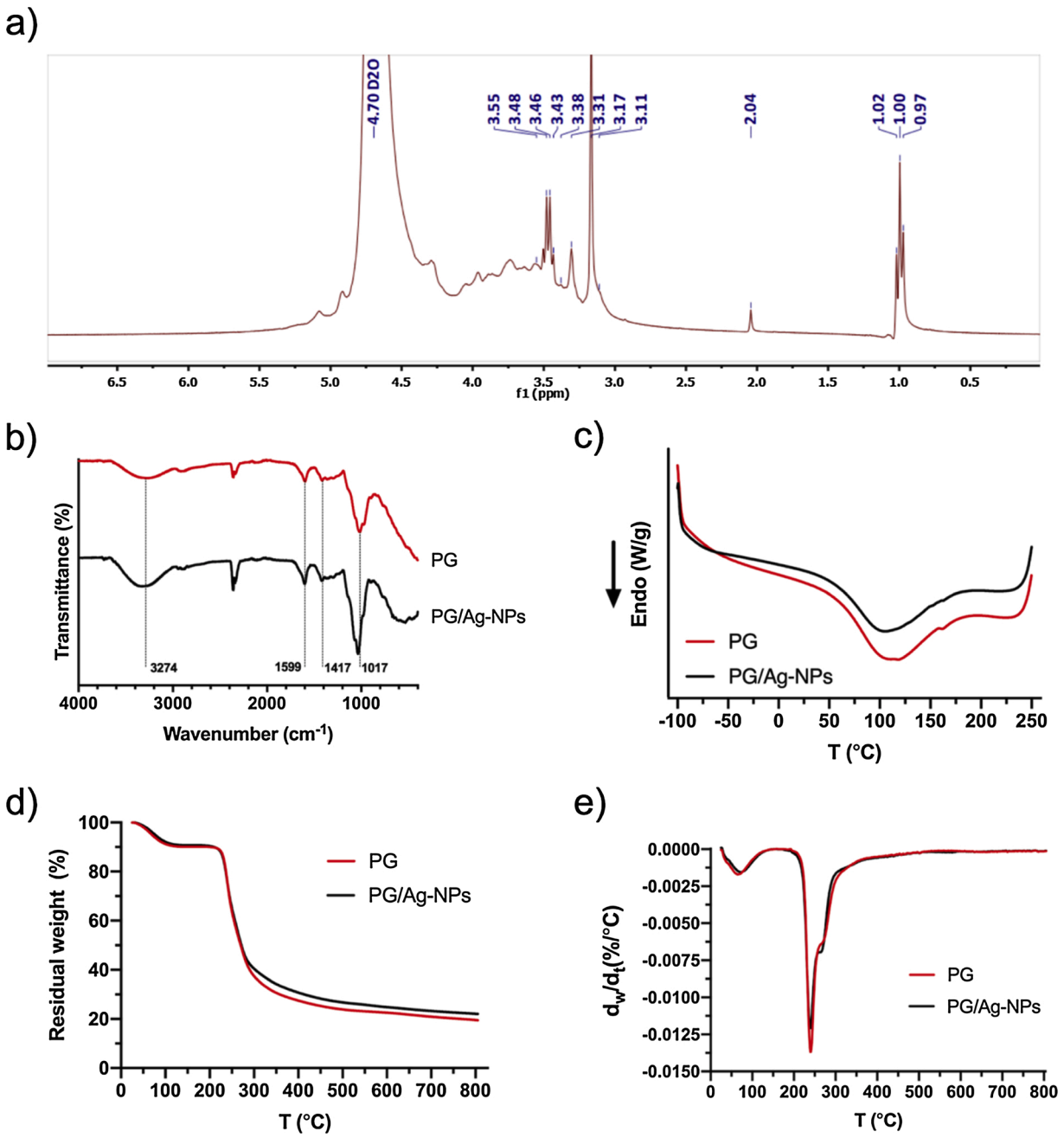

Fig. 3. (a) NMR spectra of PG, (b) PG and PG/Ag-NPs FTIR spectra, (c) DSC, (d) TGA, and (e) DTG analysis.

were observed at 4.3 and 4.9 ppm related to the glucose and galactose monosaccharides, respectively. All the aforementioned picks were in agreement with previous works (Fig. 3a) [43].

In the FTIR spectrum of PG, the absorbance bands observed at 3274 cm^{-1}, 1599 cm^{-1}, 1417 cm^{-1}, and 1017 cm^{-1} are related to hydroxyl, carboxyl, carboxylate of uronic acid residues, and C–O or C—C functional groups, respectively (Fig. 3b). After reaction and Ag immobilization, all of these characteristic peaks were recorded. However, the OH stretching vibration band was intensified and shifted to 3317 cm^{-1}. Besides, the peak at 1017 cm^{-1} was shifted to 1034 cm^{-1}. These observations could be attributed to the incorporation of Ag nanoparticles in the polymer matrix [44].

The DSC thermogram of PG showed two endothermic peaks at 107.33 °C and 161.36 °C, which are related to the melting of PG crystalline structures (Tm) (Fig. 3c). For the PG/Ag-NPs, observed Tm was slightly shifted to a lower temperature (103.07 and 161.99 °C). More interestingly, the melting enthalpy (ΔHm) of crystalline structures for PG/Ag-NPs was 313.35 J/g, which is lower than pure PG (352.30 J/g). Besides, the melting peak was broadened for PG/AG-NPs that is an indicator of a change in crystals orders [45]. Nanoparticles are capable of interacting with the polymer chain through hydrogen bonding and van der Waals forces [46]. Thus, in the presence of Ag nanoparticles, the initial crystalline structure of PG is disrupted and Ag nanoparticles hindered PG for the creation of larger crystals with higher thermal stability.

The thermal stability of the materials was also characterized using TGA (Fig. 3d). Both PG and PG/Ag-NPs had similar trends with one mass loss in the range of 35–135 °C as a result of water evaporation. The second mass loss was sharper and started near 225 °C for both samples, which is attributed to the thermal decomposition of materials. At the highest temperature (800 °C), the remaining weights for PG and PG/Ag-NPs were 19.50 % and 22.02 %, respectively. This weight difference

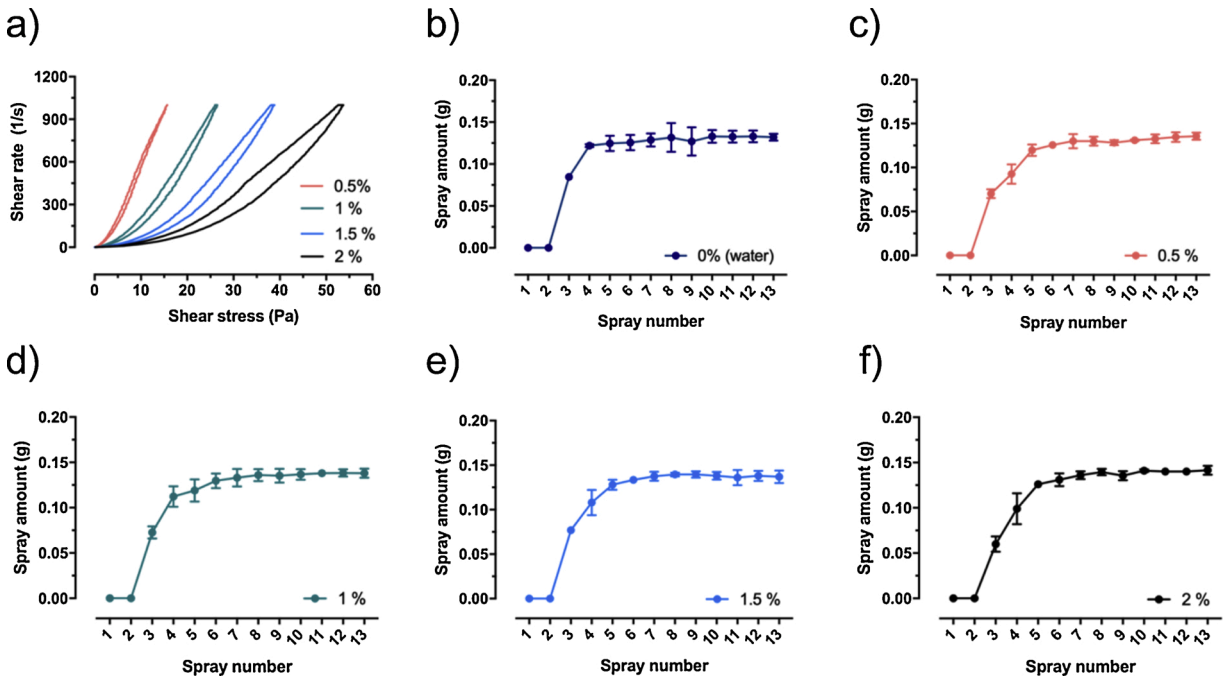

Fig. 4. (a) Rheological properties of different concentration of PG/Ag-NPs solutions, and (b-f) sprayability of pure water and different concentration of PG/Ag-NPs solutions.

between PG and PG/Ag-NPs (2.52 %) is due to the incorporation of silver in the structure and approximately shows the total embedded Ag-NPs in the structure, which is consistent with EDX results. Analysis of DTG, however, revealed that for PG/Ag-NPs the intensity of the primary decomposition rate peak is reduced, and a more significant shoulder is appeared, which reconfirms that Ag-NPs could alter the crystalline structure of PG (Fig. 3e) [47].

3.2. Rheological properties and sprayability

Rheological characterization of spray solutions was investigated by the hysteresis test. As demonstrated in Fig. 4a, the spray solutions shear stress was increased by increasing in shear rate. After that, by decreasing the shear rate, this process was reversed, and the shear stress was decreased. However, an obvious gap between the increasing and decreasing curves were recorded, which is the typical behavior for thixotropic materials [48]. Thixotropic behavior is highly favorable because it results in a decrease in viscosity upon applying force (shear thinning behavior), which enhances the sprayability. On the other hand, after spraying, the viscosity increases, and gel relaxes, allowing it to better attach to the skin surface [48].

Furthermore, the sprayability of the PG/Ag-NPs solutions was investigated to evaluate their potential application as sprayable dressings (Fig. 4b–f). The obtained results revealed that the sprayed amounts after equilibrium state for PG/Ag-NPs solutions were approximately equal to pure water (~ 0.14 g). This could be the result of their thixotropic behavior, as described in the previous section. However, there is a slight difference in the equilibrium state in which pure water reaches the equilibrium after the fourth spray, and the PG/Ag-NPs reach equilibrium after the fifth or sixth spray, which could attribute to the difference in their viscosity.

3.3. Film-forming properties

The film-forming capacity is a desirable characteristic because it shows that antibacterial sprayable dressing has the ability to cover the skin surface and prevent bacterial invasion into the wound area. Inappropriate film-forming capacity would result in cracks and open gaps on the surface in which let the bacteria to penetrate into the wound site and cause infection. The SEM photographs from the surface of the sprayed PG/Ag-NPs were recorded to investigate the formation of any undesired micro-sized fractures. As depicted in Fig. 2a and b, the sprayed dressings formed a uniform and defect-less film with no obvious cracks (hundred nanometers or micrometers size).

3.4. Stability evaluation

The result of UV–vis spectra 3 and 6 months after the initially recorded data did not exhibit a significant change in the characteristic peak wavelength or intensity (Fig. 1c). Similarly, the obtained results of

Table 1
The MIC results for PG/Ag-NPs and chloramphenicol against *S. aureus* and *P. aeruginosa*.

PG/Ag-NPs (mg/mL)	*S. aureus*	*P. aeruginosa*	Chloramphenicol (μg/mL)	*S. aureus*	*P. aeruginosa*
4.5	-	-	45	-	-
2.25	-	-	22.5	-	-
1.125	-	+	11.25	-	+
0.562	+	+	5.625	-	+
0.281	+	+	2.812	-	+
0.141	+	+	1.410	-	+
0.070	+	+	0.700	+	+
0.035	+	+	0.352	+	+

"+" bacterial growth > 10 %, "–" bacterial growth <.10 %.

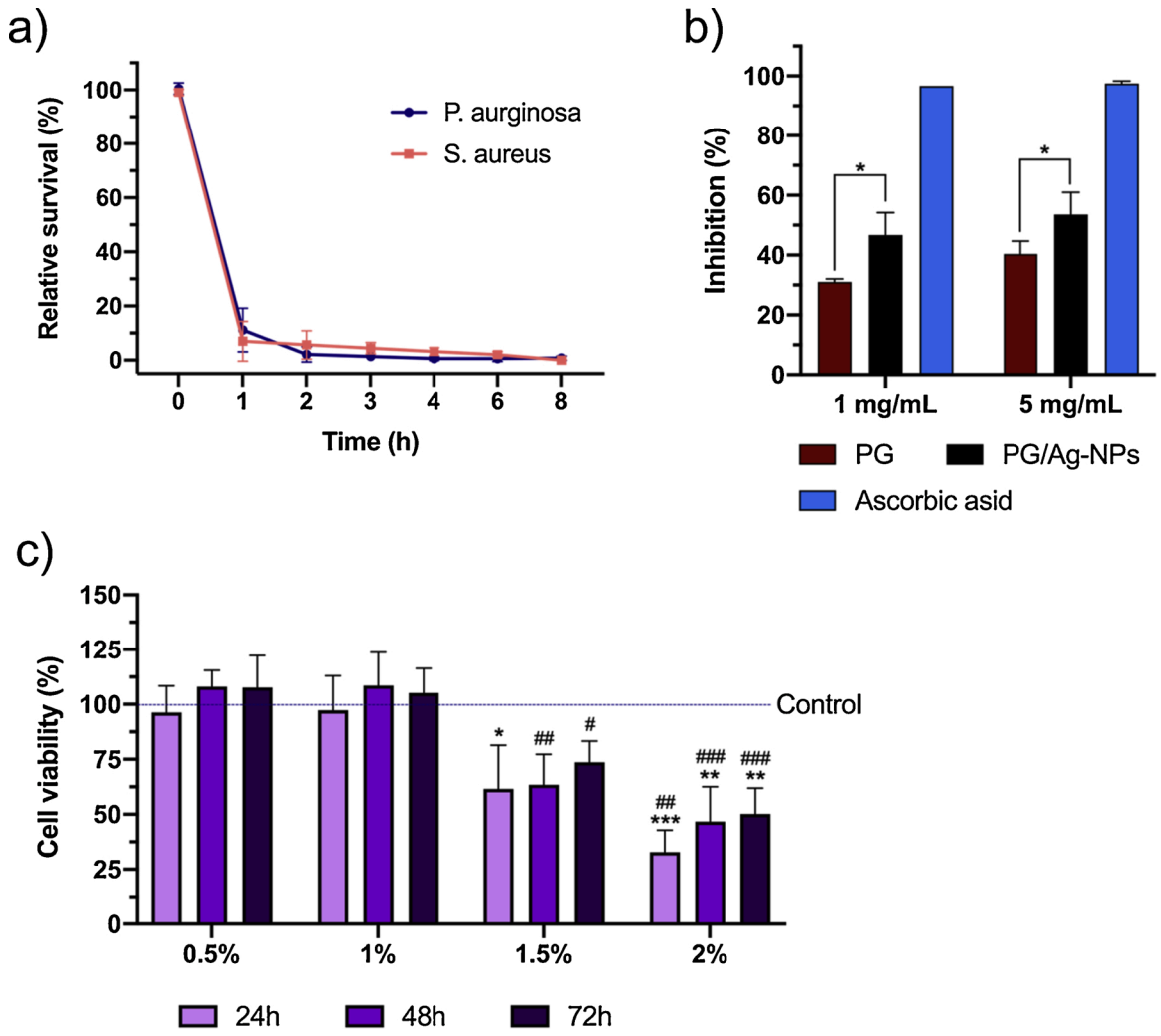

Fig. 5. (a) Kinetic assay (b) DDPH radical scavenging assay for PG and PG/Ag-NPs and (c) indirect MTT assay for different concentration of PG/Ag-NPs solutions while (*) and (#) refers to the statistical analysis compared to the control group and 1% PG/Ag-NPs respectively.

pH value measurement did not show any significant change at the same time points (Supplementary File; Fig. S1). Moreover, there was no sign of precipitation in the stored spray solutions that was expected as zeta potential results demonstrated well stability for PG/Ag-NPs suspension (Supplementary File; Fig. S2). All of these findings accentuated suitable physical and chemical stability of the fabricated sprayable dressings over the experimented period.

3.5. Antibacterial properties

Previous reports have demonstrated that Ag-NPs possess biocidal properties through disrupting bacteria's metabolism and destroying their membrane [39]. In this study, the MIC assay was implemented to investigate the biocidal properties of synthesized PG/Ag-NPs and its minimum effective concentration. The MIC value of chloramphenicol was also investigated for comparison. The results demonstrated that solutions contained 1.125 and 2.25 mg/mL of PG/Ag-NPs were capable of killing more than 90 % of *S. aureus* and *P. aeruginosa,* respectively (Table 1).

Furthermore, a time-dependent response of both bacteria in contact with 1% PG-Ag/NPs was recorded. As represented in Fig. 5a, the fractional survival of both bacteria was significantly decreased (<10 %) only after one hour of incubation. For *P. aeruginosa* bacteria, survival reached zero after 3 h, while for *S. aureus* bacteria, survival reached zero after 8 h (Supplementary File; Fig. S3).

Previous works have also shown the antibacterial performance of Ag nanoparticles [49]. For instance, Xie et al. developed chitosan-Ag nanoparticle hydrogels for wound healing. They showed that incorporation of Ag nanoparticles increased the antibacterial activity of the chitosan hydrogels to reach inhibition rates of > 99 % for *E. Coli* and *S. aureus* after 24 h. However, they used significantly higher concentrations of Ag compared to this work.

3.6. Antioxidant and cytotoxicity properties

As shown in Fig. 5b, extracted PG demonstrated good radical scavenging ability while its ability improves by increasing concentration. Moreover, the radical scavenging was significantly improved (*$p < 0.05$) in PG/Ag-NPs compared to PG. That could be the result of the radical scavenging capacity of the synthesized Ag-NPs, which is in agreement with previous studies [50].

Furthermore, *in vitro* cytotoxicity assay demonstrated that PG/Ag-NPs, at concentrations less than 1%, not only did not cause any cytotoxicity but also slightly improved the proliferation of fibroblast cells (Fig. 5c). However, cell viability was significantly decreased at 1.5 and 2 % PG/Ag-NPs. By increasing the solutions' viscosity, cells did not receive their primary nutrition due to the reduction in nutrient transfer rate [51]. Besides, the cytotoxicity effect of Ag-NPs at higher concentrations could be another reason for this observation [1].

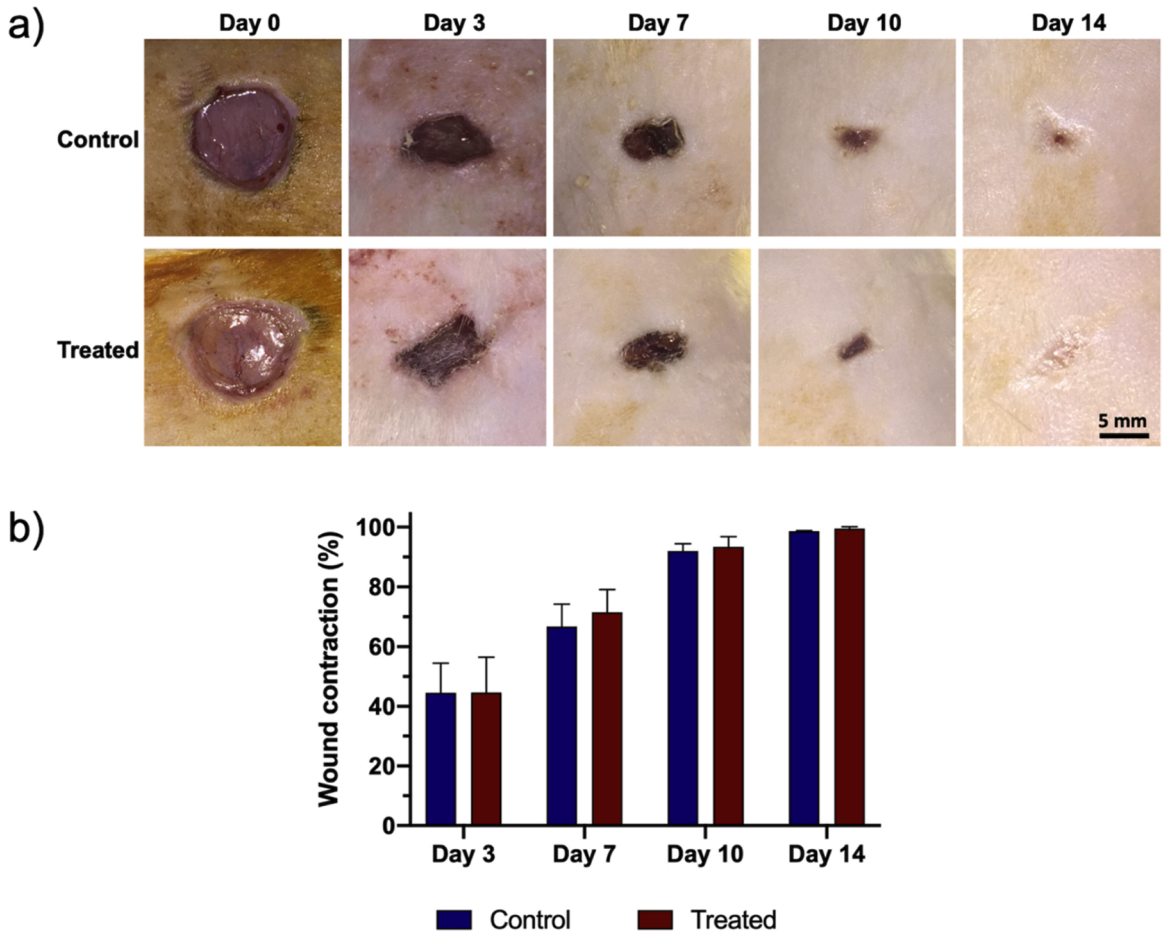

Fig. 6. (a) Macroscopic images of wound closure at different time intervals for untreated (control) and PG/Ag-NPs treated groups and (b) wound closure rate for untreated and PG/Ag-NPs treated groups.

3.7. *In vivo study*

The PG/Ag-NPs 1% was selected as an optimum concentration for *in vivo* analysis because, at this concentration, the solution exhibited proper rheological and sprayability properties, proper bactericidal characteristics, and no cytotoxic effect on fibroblasts cells. Furthermore, its *in vivo* biocompatibility and wound healing properties were investigated by both macroscopic and histological evaluations. The macroscopic images of wound healing during a two-week period were shown in Fig. 6a. Results showed that PG/Ag-NPs treated groups were completely healed after 14 days with no sign of scar formation. Moreover, quantitative calculation of wound contraction revealed that PG/Ag-NPs treated groups slightly improve wound contraction (Fig. 6b).

The histological results after 3-days post-surgery showed full-thickness necrosis with an inflammatory response in all groups (Fig. 7a). Moreover, while early granulation tissue was formed in both groups, no re-epithelization was observed before the 7th day. After 7-days, the inflammatory response was observed to be lower for the treated group than the control. Moreover, the formation of the epithelium was evident in the treated group while it was significantly weaker in the control group. 10-days post-surgery, the inflammatory cells were still more abundant in the control group. At this time-point, re-epithelization in the treated group continued to form an almost complete epithelium. However, for the control, re-epithelization was obvious but not complete, which could be the result of its more severe inflammatory response [52]. After 14-days, re-epithelization was complete in both groups; however, the treated group demonstrated a more mature re-epithelization comparably. Additionally, in both groups, the inflammatory response was decreased over time, and mature granulation tissue was formed. It is known that high collagen deposition by myofibroblasts within the wound site results in scar tissue formation [6]. Hence, Masson's trichrome staining was used to investigate collagen formation and deposition (Fig. 7b). Based on the results, the treated groups did not show any significant increase in collagen formation and deposition compared to the control group. This is advantageous since formulated sprays do not intend to increase scar formation. These observations confirmed that formulated sprayable dressings are capable of enhancing wound healing by better re-epithelization and normal collagen deposition.

4. Conclusion

In this work, attempts were made to synthesize and develop new formulations for antibacterial wound dressing. On this demand, Persian gum (PG) were isolated and used to fabricate Ag-nanoparticles embedded PG (PG/Ag-NPs). PG/Ag-NPs were successfully synthesized using a facile method with high efficiency. The presence of silver nanoparticles was confirmed by UV/Vis spectroscopy, EDX, and TEM images, and nanoparticles were found to have a diameter of 5.6 $\pm$ 1.0 nm. Moreover, DSC and TGA analysis showed that Ag immobilization altered the crystalline structure of PG and changed the stability of these structures. Four different spray solutions were prepared, and the effect of PG/Ag-NPs concentration (0.5, 1, 1.5, and 2 wt.%) on spray properties was investigated. Results showed that all formulations possess a thixotropic behavior, sprayed easily and reach a steady spraying amount, and form defectless films after solvent evaporation. For the

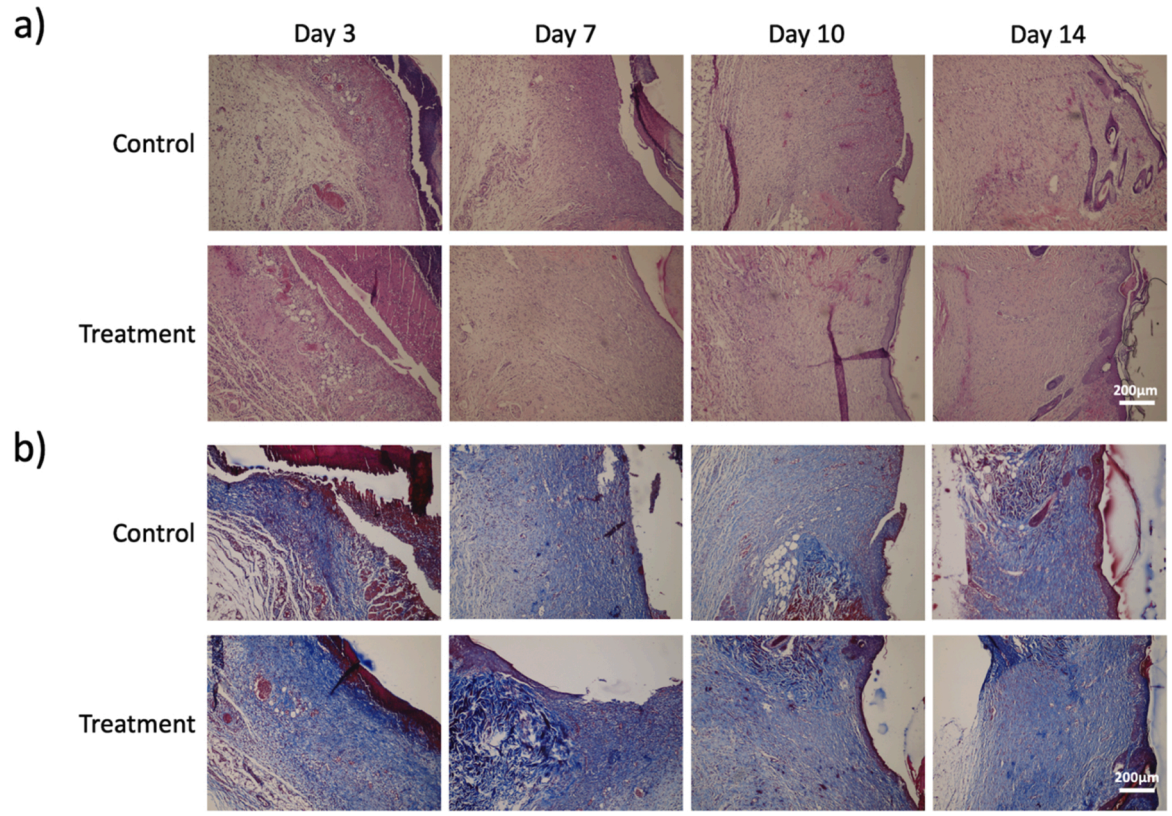

Fig. 7. Histological examination of wound cites with a) H&E Staining and b) Masson's Trichrome Staining at different times.

tested period (six months), formulations also showed no signs of precipitation or change in pH value and UV/vis absorbance peak, confirming their long shelf life. In addition, the antibacterial tests revealed high bactericidal efficiency of the optimum spray formulation (1%) against both gram-positive *S. aureus* and gram-negative *P. aeruginosa* while the MTT assay revealed that this PG/Ag-NPs concentration could accelerate fibroblast proliferation. Finally, while the macroscopic evaluation of *in vivo* full-thickness wound healing exhibited no significant difference, the histological investigation demonstrated reduced inflammatory response and enhanced re-epithelization in the treated group.

Declaration of Competing Interest

The authors report no declarations of interest.

Acknowledgments

S.-S. Hashemi acknowledges the financial support from Shiraz University of Medical Sciences (grant no. 23695). M.-A. Shahbazi acknowledges the financial support from the Academy of Finland (grant no. 317316).

Appendix A. Supplementary data

Supplementary data associated with this article can be found, in the online version, at https://doi.org/10.1016/j.mtcomm.2021.102225.

References

[1] A. Amirsadeghi, A. Jafari, L.J. Eggermont, S.S. Hashemi, S.A. Bencherif, M. Khorram, Vascularization strategies for skin tissue engineering, Biomater. Sci. 8 (2020) 4052–4073, https://doi.org/10.1039/d0bm00266f.

[2] Y. Zhao, Z. Li, S. Song, K. Yang, H. Liu, Z. Yang, J. Wang, B. Yang, Q. Lin, Skin-inspired antibacterial conductive hydrogels for epidermal sensors and diabetic foot wound dressings, Adv. Funct. Mater. 29 (2019) 1901474, https://doi.org/10.1002/adfm.201901474.

[3] G.H.R. Ceilley, Chronic wound healing: a review of current management and treatments, Adv. Ther. 34 (2021), https://doi.org/10.1007/s12325-017-0478-y (n. d.).

[4] N.T. Thet, J. Mercer-Chalmers, R.J. Greenwood, A.E.R. Young, K. Coy, S. Booth, A. Sack, A.T.A. Jenkins, SPaCE swab: point-of-care sensor for simple and rapid detection of acute wound infection, ACS Sens. 5 (2020) 2652–2657, https://doi.org/10.1021/acssensors.0c01265.

[5] M. Mahmoudi, L. Gould, Opportunities and challenges of the management of chronic wounds: a multidisciplinary viewpoint, Chronic Wound Care Manage. Res. 7 (2020) 27–36, https://doi.org/10.2147/cwcmr.s260136.

[6] A. Jafari, A. Amirsadeghi, S. Hassanajili, N. Azarpira, Bioactive antibacterial bilayer PCL/gelatin nanofibrous scaffold promotes full-thickness wound healing, Int. J. Pharm. 583 (2020) 119413, https://doi.org/10.1016/j.ijpharm.2020.119413.

[7] M.J. Pestrak, P. Baker, S. Dellos-Nolan, P.J. Hill, D. Passos da Silva, H. Silver, I. Lacdao, D. Raju, M.R. Parsek, D.J. Wozniak, P. Lynne Howell, Treatment with the pseudomonas aeruginosa glycoside hydrolase PslG combats wound infection by improving antibiotic efficacy and host innate immune activity, Antimicrob. Agents Chemother. 63 (2019), https://doi.org/10.1128/AAC.00234-19.

[8] G. Norman, J.C. Dumville, D.P. Mohapatra, G.L. Owens, E.J. Crosbie, Antibiotics and antiseptics for surgical wounds healing by secondary intention, Cochrane Database Syst. Rev. 2016 (2016), https://doi.org/10.1002/14651858.CD011712.pub2.

[9] Y. Ma, L. Xin, H. Tan, M. Fan, J. Li, Y. Jia, Z. Ling, Y. Chen, X. Hu, Chitosan membrane dressings toughened by glycerol to load antibacterial drugs for wound healing, Mater. Sci. Eng. C 81 (2017) 522–531, https://doi.org/10.1016/j.msec.2017.08.052.

[10] N.T. Ardekani, M. Khorram, K. Zomorodian, S. Yazdanpanah, H. Veisi, H. Veisi, Evaluation of electrospun poly (vinyl alcohol)-based nanofiber mats incorporated with Zataria multiflora essential oil as potential wound dressing, Int. J. Biol. Macromol. 125 (2019) 743–750, https://doi.org/10.1016/j.ijbiomac.2018.12.085.

[11] A. Jafari, S. Hassanajili, M.B. Karimi, A. Emami, F. Ghaffari, N. Azarpira, Effect of organic/inorganic nanoparticles on performance of polyurethane nanocomposites for potential wound dressing applications, J. Mech. Behav. Biomed. Mater. 88 (2018) 395–405, https://doi.org/10.1016/j.jmbbm.2018.09.001.

[12] J. Yang, K. Wang, D.G. Yu, Y. Yang, S.W.A. Bligh, G.R. Williams, Electrospun Janus nanofibers loaded with a drug and inorganic nanoparticles as an effective antibacterial wound dressing, Mater. Sci. Eng. C 111 (2020) 110805, https://doi.org/10.1016/j.msec.2020.110805.

[13] R.M. Abdelrahman, A.M. Abdel-Mohsen, M. Zboncak, J. Frankova, P. Lepcio, L. Kobera, M. Steinhart, D. Pavlinak, Z. Spotaz, R. Sklenářévá, J. Brus, J. Jancar, Hyaluronan biofilms reinforced with partially deacetylated chitin nanowhiskers:

extraction, fabrication, in-vitro and antibacterial properties of advanced nanocomposites, Carbohydr. Polym. 235 (2020) 115951, https://doi.org/10.1016/j.carbpol.2020.115951.
[14] S. Homaeigohar, A.R. Boccaccini, Antibacterial biohybrid nanofibers for wound dressings, Acta Biomater. 107 (2020) 25–49, https://doi.org/10.1016/j.actbio.2020.02.022.
[15] N. Tra Thanh, M. Ho Hieu, N. Tran Minh Phuong, T. Do Bui Thuan, H. Nguyen Thi Thu, V.P. Thai, T. Do Minh, H. Nguyen Dai, V.T. Vo, H. Nguyen Thi, Optimization and characterization of electrospun polycaprolactone coated with gelatin-silver nanoparticles for wound healing application, Mater. Sci. Eng. C 91 (2018) 318–329, https://doi.org/10.1016/j.msec.2018.05.039.
[16] J.X. Liu, W.H. Dong, X.J. Mou, G.S. Liu, X.W. Huang, X. Yan, C.F. Zhou, S. Jiang, Y. Z. Long, In situ electrospun zein/thyme essential oil-based membranes as an effective antibacterial wound dressing, ACS Appl. Bio Mater. 3 (2020) 302–307, https://doi.org/10.1021/acsabm.9b00823.
[17] J. Qu, X. Zhao, Y. Liang, Y. Xu, P.X. Ma, B. Guo, Degradable conductive injectable hydrogels as novel antibacterial, anti-oxidant wound dressings for wound healing, Chem. Eng. J. 362 (2019) 548–560, https://doi.org/10.1016/j.cej.2019.01.028.
[18] N. Boonmak, J. Niyompanich, P. Chuysinuan, P. Niamlang, P. Ekabutr, P. Supaphol, Preparation of mangosteen extract-loaded poly(vinyl acetate) for use as an antibacterial spray-on dressing, J. Drug Deliv. Sci. Technol. 46 (2018) 322–329, https://doi.org/10.1016/j.jddst.2018.05.033.
[19] S. Tavakoli, H. Mokhtari, M. Kharaziha, A. Kermanpur, A. Talebi, J. Moshtaghian, A multifunctional nanocomposite spray dressing of Kappa-carrageenan-polydopamine modified ZnO/L-glutamic acid for diabetic wounds, Mater. Sci. Eng. C 111 (2020) 110837, https://doi.org/10.1016/j.msec.2020.110837.
[20] D.S. Yoon, Y. Lee, H.A. Ryu, Y. Jang, K.M. Lee, Y. Choi, W.J. Choi, M. Lee, K. M. Park, K.D. Park, J.W. Lee, Cell recruiting chemokine-loaded sprayable gelatin hydrogel dressings for diabetic wound healing, Acta Biomater. 38 (2016) 59–68, https://doi.org/10.1016/j.actbio.2016.04.030.
[21] N. Annabi, D. Rana, E. Shirzaei Sani, R. Portillo-Lara, J.L. Gifford, M.M. Fares, S. M. Mithieux, A.S. Weiss, Engineering a sprayable and elastic hydrogel adhesive with antimicrobial properties for wound healing, Biomaterials 139 (2017) 229–243, https://doi.org/10.1016/j.biomaterials.2017.05.011.
[22] K. Kathe, H. Kathpalia, Film forming systems for topical and transdermal drug delivery, Asian J. Pharm. Sci. 12 (2017) 487–497, https://doi.org/10.1016/j.ajps.2017.07.004.
[23] H. Ghasemzadeh, F. Modiri, Application of novel Persian gum hydrocolloid in soil stabilization, Carbohydr. Polym. 246 (2020) 116639, https://doi.org/10.1016/j.carbpol.2020.116639.
[24] M. Dabestani, R. Kadkhodaee, G.O. Phillips, S. Abbasi, Persian gum: a comprehensive review on its physicochemical and functional properties, Food Hydrocoll. 78 (2018) 92–99, https://doi.org/10.1016/j.foodhyd.2017.06.006.
[25] M. Hadian, S.M.H. Hosseini, A. Farahnaky, G.R. Mesbahi, Optimization of functional nanoparticles formation in associative mixture of water-soluble portion of Farsi gum and beta-lactoglobulin, Int. J. Biol. Macromol. 102 (2017) 1297–1303, https://doi.org/10.1016/j.ijbiomac.2017.05.022.
[26] F. Sadeghi, R. Kadkhodaee, B. Emadzadeh, G.O. Phillips, Phase behavior, rheological characteristics and microstructure of sodium caseinate-Persian gum system, Carbohydr. Polym. 179 (2018) 71–78, https://doi.org/10.1016/j.carbpol.2017.09.060.
[27] M. Sepeidnameh, S.M.H. Hosseini, M. Niakosari, G.R. Mesbahi, G.H. Yousefi, M. T. Golmakani, M. Nejadmansouri, Physicochemical properties of fish oil in water multilayer emulsions prepared by a mixture of whey protein isolate and water-soluble fraction of Farsi gum, Int. J. Biol. Macromol. 118 (2018) 1639–1647, https://doi.org/10.1016/j.ijbiomac.2018.07.007.
[28] N. Behera, M. Arakha, M. Priyadarshinee, B.S. Pattanayak, S. Soren, S. Jha, B. C. Mallick, Oxidative stress generated at nickel oxide nanoparticle interface results in bacterial membrane damage leading to cell death, RSC Adv. 9 (2019) 24888–24894, https://doi.org/10.1039/c9ra02082a.
[29] X. Pan, Y. Wang, Z. Chen, D. Pan, Y. Cheng, Z. Liu, Z. Lin, X. Guan, Investigation of antibacterial activity and related mechanism of a series of nano-Mg(OH)2, ACS Appl. Mater. Interfaces 5 (2013) 1137–1142, https://doi.org/10.1021/am302910q.
[30] Z. Lu, J. Gao, Q. He, J. Wu, D. Liang, H. Yang, R. Chen, Enhanced antibacterial and wound healing activities of microporous chitosan-Ag/ZnO composite dressing, Carbohydr. Polym. 156 (2017) 460–469, https://doi.org/10.1016/j.carbpol.2016.09.051.
[31] S. Sanyasi, R.K. Majhi, S. Kumar, M. Mishra, A. Ghosh, M. Suar, P.V. Satyam, H. Mohapatra, C. Goswami, L. Goswami, Polysaccharide-capped silver Nanoparticles inhibit biofilm formation and eliminate multi-drug-resistant bacteria by disrupting bacterial cytoskeleton with reduced cytotoxicity towards mammalian cells, Sci. Rep. 6 (2016) 1–16, https://doi.org/10.1038/srep24929.
[32] M.K. Rai, S.D. Deshmukh, A.P. Ingle, A.K. Gade, Silver nanoparticles: the powerful nanoweapon against multidrug-resistant bacteria, J. Appl. Microbiol. 112 (2012) 841–852, https://doi.org/10.1111/j.1365-2672.2012.05253.x.
[33] S.P. Deshmukh, S.M. Patil, S.B. Mullani, S.D. Delekar, Silver nanoparticles as an effective disinfectant: a review, Mater. Sci. Eng. C 97 (2019) 954–965, https://doi.org/10.1016/j.msec.2018.12.102.
[34] T. Maneerung, S. Tokura, R. Rujiravanit, Impregnation of silver nanoparticles into bacterial cellulose for antimicrobial wound dressing, Carbohydr. Polym. 72 (2008) 43–51, https://doi.org/10.1016/j.carbpol.2007.07.025.
[35] H. Choudhury, M. Pandey, Y.Q. Lim, C.Y. Low, C.T. Lee, T.C.L. Marilyn, H.S. Loh, Y.P. Lim, C.F. Lee, S.K. Bhattamishra, P. Kesharwani, B. Gorain, Silver nanoparticles: advanced and promising technology in diabetic wound therapy, Mater. Sci. Eng. C 112 (2020) 110925, https://doi.org/10.1016/j.msec.2020.110925.
[36] J. Song, H. Kang, C. Lee, S.H. Hwang, J. Jang, Aqueous synthesis of silver nanoparticle embedded cationic polymer nanofibers and their antibacterial activity, ACS Appl. Mater. Interfaces 4 (2012) 460–465, https://doi.org/10.1021/am201563t.
[37] H. Lv, S. Cui, Q. Yang, X. Song, D. Wang, J. Hu, Y. Zhou, Y. Liu, AgNPs-incorporated nanofiber mats: Relationship between AgNPs size/content, silver release, cytotoxicity, and antibacterial activity, Mater. Sci. Eng. C. 118 (2021) 111331, https://doi.org/10.1016/j.msec.2020.111331.
[38] S.V. Niknezhad, G. Najafpour Darzi, S. Kianpour, S. Jafarzadeh, H. Mohammadi, Y. Ghasemi, R. Heidari, M.A. Shahbazi, Bacteria-assisted biogreen synthesis of radical scavenging exopolysaccharide-iron complexes: an oral nano-sized nutritional supplement with high: in vivo compatibility, J. Mater. Chem. B 7 (2019) 5211–5221, https://doi.org/10.1039/c9tb01077g.
[39] P. Senthilkumar, G. Yaswant, S. Kavitha, E. Chandramohan, G. Kowsalya, R. Vijay, B. Sudhagar, D.S.R.S. Kumar, Preparation and characterization of hybrid chitosan-silver nanoparticles (Chi-Ag NPs); A potential antibacterial agent, Int. J. Biol. Macromol. 141 (2019) 290–297, https://doi.org/10.1016/j.ijbiomac.2019.08.234.
[40] M. Kim, J.W. Byun, D.S. Shin, Y.S. Lee, Spontaneous formation of silver nanoparticles on polymeric supports, Mater. Res. Bull. 44 (2009) 334–338, https://doi.org/10.1016/j.materresbull.2008.05.014.
[41] K. Zhu, S.R. Shin, T. van Kempen, Y.-C. Li, V. Ponraj, A. Nasajpour, S. Mandla, N. Hu, X. Liu, J. Leijten, Y.-D. Lin, M.A. Hussain, Y.S. Zhang, A. Tamayol, A. Khademhosseini, Gold nanocomposite bioink for printing 3D cardiac constructs, Adv. Funct. Mater. 27 (2017) 1605352, https://doi.org/10.1002/adfm.201605352.
[42] X. Zhuang, B. Cheng, W. Kang, X. Xu, Electrospun chitosan/gelatin nanofibers containing silver nanoparticles, Carbohydr. Polym. 82 (2010) 524–527, https://doi.org/10.1016/j.carbpol.2010.04.085.
[43] G. Fadavi, M. Ghiasi, A. Zargarran, M.A. Mohammadifar, Some physicochemical and rheological properties of Zedo (Farsi) gum exudates from Amygdalus scoparia, Nutr. Food Sci. Res. 4 (2017) 33–40, https://doi.org/10.18869/acadpub.nfsr.4.1.33.
[44] M. Dabestani, R. Kadkhodaee, G.O. Phillips, S. Abbasi, Persian gum: a comprehensive review on its physicochemical and functional properties, Food Hydrocoll. 78 (2018) 92–99, https://doi.org/10.1016/j.foodhyd.2017.06.006.
[45] M.B. Karimi, S. Hassanajili, Short fiber/polyurethane composite membrane for gas separation, J. Memb. Sci. 543 (2017) 40–48, https://doi.org/10.1016/j.memsci.2017.08.043.
[46] N. Cai, Q. Dai, Z. Wang, X. Luo, Y. Xue, F. Yu, Toughening of electrospun poly(l-lactic acid) nanofiber scaffolds with unidirectionally aligned halloysite nanotubes, J. Mater. Sci. 50 (2015) 1435–1445, https://doi.org/10.1007/s10853-014-8703-4.
[47] G. Fadavi, M.A. Mohammadifar, A. Zargarran, A.M. Mortazavian, R. Komeili, Composition and physicochemical properties of Zedo gum exudates from Amygdalus scoparia, Carbohydr. Polym. 101 (2014) 1074–1080, https://doi.org/10.1016/j.carbpol.2013.09.095.
[48] K.J. Geh, A. Stelzl, A. Gröne, L. Wagner, B. Förster, G. Winter, Development of a sprayable hydrogel formulation for the skin application of therapeutic antibodies, Eur. J. Pharm. Biopharm. 142 (2019) 123–132, https://doi.org/10.1016/j.ejpb.2019.06.015.
[49] Y. Xie, X. Liao, J. Zhang, F. Yang, Z. Fan, Novel chitosan hydrogels reinforced by silver nanoparticles with ultrahigh mechanical and high antibacterial properties for accelerating wound healing, Int. J. Biol. Macromol. 119 (2018) 402–412, https://doi.org/10.1016/j.ijbiomac.2018.07.060.
[50] Y.K. Mohanta, S.K. Panda, R. Jayabalan, N. Sharma, A.K. Bastia, T.K. Mohanta, Antimicrobial, antioxidant and cytotoxic activity of silver nanoparticles synthesized by leaf extract of Erythrina suberosa (Roxb.), Front. Mol. Biosci. 4 (2017) 14, https://doi.org/10.3389/fmolb.2017.00014.
[51] J. Jia, D.J. Richards, S. Pollard, Y. Tan, J. Rodriguez, R.P. Visconti, T.C. Trusk, M. J. Yost, H. Yao, R.R. Markwald, Y. Mei, Engineering alginate as bioink for bioprinting, Acta Biomater. 10 (2014) 4323–4331, https://doi.org/10.1016/j.actbio.2014.06.034.
[52] A. Jafari, S. Hassanajili, N. Azarpira, M. Bagher Karimi, B. Geramizadeh, Development of thermal-crosslinkable chitosan/maleic terminated polyethylene glycol hydrogels for full thickness wound healing: in vitro and in vivo evaluation, Eur. Polym. J. 118 (2019) 113–127, https://doi.org/10.1016/j.eurpolymj.2019.05.046.